

## MAJOR TRANSITION-METAL OXIDE MINERALS: THEIR ELECTRONIC STRUCTURES AND THE INTERPRETATION OF MINERALOGICAL PROPERTIES

DAVID J. VAUGHAN

*Department of Geological Sciences, University of Aston in Birmingham,  
Birmingham B4 7ET, England*

JOHN A. TOSSELL

*Department of Chemistry, University of Maryland, College Park, Maryland 20742, U.S.A.*

### ABSTRACT

Simplified electronic-structure models based on molecular orbital calculations are presented for hematite, magnetite, ilmenite, ulvöspinel and chromite. The "one-electron" MO/band-theory models are correlated with the properties of these minerals. Spectral reflectivity variations are interpreted from the energies of *allowed* electronic transitions involving both orbitals dominantly metal in character and those dominantly oxygen. The influence of electronic structure on limits of solid solution, Vickers hardness and thermochemical properties is also considered. In particular, the contribution to stability of the main bonding orbitals (chiefly metal  $3d$  and oxygen  $2p$  in character) is assessed. The electronic structures and mineral properties of wüstite, rutile and eskolaite are also briefly reviewed.

### SOMMAIRE

Des modèles simplifiés de structure électronique fondés sur le calcul d'orbitales moléculaires sont présentés pour l'hématite, la magnétite, l'ilménite, l'ulvöspinel et la chromite. On établit une corrélation entre ces modèles et les propriétés des minéraux considérés. Les variations en réflectivité spectrale s'expliquent à partir des énergies de transitions électroniques permises qui impliquent à la fois les orbitales à caractère nettement métallique et celles dont le caractère dépend surtout de l'oxygène. La structure électronique exerce son influence sur les limites de solution solide, la dureté Vickers et les propriétés thermochimiques; en particulier, les orbites principales de liaisons (surtout métal  $3d$  et oxygène  $2p$ ) contribuent à la stabilité. Les structures électroniques et propriétés minérales de la wüstite, du rutile et de l'eskolaïte sont passées en revue.

(Traduit par la Rédaction)

### INTRODUCTION

Electronic structure (or 'chemical bonding') models are fundamental to an understanding of

mineral properties, stabilities and occurrence, and to prediction of mineral behavior under various pressure and temperature conditions. Although a number of models of varying complexity may be proposed, we believe that an approach based on molecular orbital (MO) theory incorporating some elements of band theory is most useful to the mineralogist.

In recent years, improved methods of quantum-mechanical calculation and spectroscopic data of greater resolution have enabled more complex systems to be successfully modelled in this way. Such studies have included calculations on cluster units of transition-metal ions coordinated to oxygen (*e.g.*, Tossell *et al.* 1973, 1974; Tossell 1976a,b). Such units combine to form the petrologically important oxide minerals hematite, magnetite, ilmenite, ulvöspinel and chromite. The object of this paper is to present simplified ("one-electron") models of the electronic structures of these minerals in the valence region and to show how they may be used to understand the properties of interest to the mineralogist. In particular, the quantitative ore-microscopic properties of reflectivity and Vickers microhardness will be considered as will, where possible, the relationship between electronic structure and crystal structure, magnetic and electrical properties, thermochemistry and solid solution behavior.

The electronic structure models described here are considered as providing an adequate description of the outer (valence) electrons of the oxides, despite the complexity of the systems. As Goodenough (1963, 1971) has stated, the outer electrons in such crystalline solids can be described by two limiting theories: the crystal- (or ligand-) field theory and the band theory. In crystal-field theory, the interactions between neighboring atoms are so weak that each electron remains *localized* at a discrete atomic position; band theory assumes that the interactions are so large that each electron is shared between the nuclei

TABLE 1. IONIC RADII AND CRYSTAL FIELD DATA FOR TRANSITION METAL IONS IN OXIDES

| Ion and Coordination | Ionic Radius (Å) (1) | Number of 3d electrons | Crystal Field Stabilization Energy (kcal/mol) (2) | Spectroscopic Data on Crystal Field Splitting (3)   |
|----------------------|----------------------|------------------------|---|---|
| Fe <sup>3+</sup> oct | 0.645                | 5                      | 0   | hematite ${}^6A_{1g} \rightarrow {}^4T_{1g}, {}^4T_{2g}$ ; 11,630cm <sup>-1</sup> (1.44 ev) |
| Fe <sup>2+</sup> oct | 0.78                 | 6                      | 11.9  | "spinel oxide"<br>${}^3T_{2g} \rightarrow {}^5E$ ; 10,000cm <sup>-1</sup> (950nm, 1.24 ev)  |
| Ti <sup>4+</sup> oct | 0.605                | 0                      | 0   |   |
| Fe <sup>2+</sup> tet | 0.63                 | 6                      | 7.9   | "spinel oxide"<br>${}^3E \rightarrow {}^5T_2$ ; 5,000cm <sup>-1</sup> (2000nm, 0.62 ev)     |
| Cr <sup>3+</sup> oct | 0.615                | 3                      | 53.7  | "spinel oxide"<br>${}^4A_2 \rightarrow {}^4T_2$ ; 17,700cm <sup>-1</sup> (530nm, 2.19 ev)   |
| Fe <sup>3+</sup> tet | 0.49                 | 5                      | 0   | "spinel oxide"<br>${}^6A_1 \rightarrow {}^4T_1$ ; ~16,000cm <sup>-1</sup> (~650nm, 1.98 ev) |
| Ti <sup>3+</sup> oct | 0.670                | 1                      | 20.9  |   |

(1) All ionic radii from Shannon (1976); (2) All average data from Burns (1970); (3) Hematite data from Tosell *et al.* (1973), spinel oxide data from the compilation of Mao & Bell (1975).

(i.e., delocalized). The formidable problem of describing the interactions of these "many electrons" is normally simplified to description of a single electron moving in a periodic potential.

Such "one-electron" energies can then be used to construct energy-level diagrams.

Molecular-orbital theory is capable of describing systems with valence electrons ranging from highly delocalized to highly localized, and the results of cluster unit calculations can be used to construct "one-electron" MO/band energy level diagrams. The major errors introduced by the "one-electron" treatment are those of ignoring the correlation in the motion of electrons with opposite spin (the correlation of like-spin electrons is properly treated) and in the neglect of multiplet effects.

As the oxides being considered form two distinct structural groups, hematite-ilmenite and the spinels (magnetite, chromite, ulvöspinel), they will be discussed under these divisions. The binary oxides wüstite, rutile and eskolaite, although of less direct petrological importance, are also discussed for completeness.

The relevance of interpretations based on ionic radii and on the crystal-field theory of transition metals (see Table 1) will also be critically assessed in an attempt to produce satisfactory working models.

## HEMATITE, ILMENITE AND THE HEMATITE-ILMENITE SERIES

Both hematite and ilmenite possess rhombohedral crystal structures closely related to that of

TABLE 2. STRUCTURAL, MINERALOGICAL, THERMOCHEMICAL AND ELECTRICAL/MAGNETIC DATA FOR TRANSITION METAL OXIDE MINERALS

| MINERAL  | CRYSTAL STRUCTURE DATA (1)<br>SPACE GROUP  | REFLECTIVITY (2)<br>R% AT 589nm                 | VHN AT 100g (2)               | THERMAL STABILITY (*K) (4) | $\Delta H_{298}^{(4)}$  | $\Delta G_{298}^{(4)}$  | ELECTRICAL AND MAGNETIC DATA (5)  |
|--|--|---|-------------------------------|----------------------------|---|---|---|
| Hematite<br>$\alpha\text{-Fe}_2\text{O}_3$                 | Rhomb.<br>R3c<br>$a = 5.034\text{Å}$<br>$a = 13.752\text{Å}$   | $R_{\text{Fe}} = 25.1$<br>$R_{\text{O}} = 28.8$ | 920-1062                      | 1895                       | -197.3 kcal/gfw   | -177.7 kcal/gfw   | Semiconductor (probably p-type). Antiferromagnetic ( $T_N = 963^\circ\text{K}$ ) with parasitic ferromagnetism when $250^\circ\text{K} < T < T_N$ . |
| Ilmenite<br>$\text{FeTiO}_3$                               | Rhomb.<br>R3<br>$a = 5.523\text{Å}$<br>$a = 54.51^\circ$<br>Hexagonal axes:<br>$a = 5.079\text{Å}$<br>$a = 14.135\text{Å}$ | $R_{\text{Fe}} = 17.3$<br>$R_{\text{O}} = 20.0$ | ~550-700                      | 1640                       | -295.6 kcal/gfw   | -277.1 kcal/gfw   | Semiconductor. Antiferromagnetic ( $T_N \approx 60^\circ\text{K}$ ).  |
| Magnetite<br>$\text{Fe}_3\text{O}_4$                       | Cubic<br>Fd3m<br>$a = 8.396\text{Å}$   | 20.0  | 534-577                       | 1870                       | -267.4 kcal/gfw   | -243.1 kcal/gfw   | Semiconductor. Ferrimagnetic ( $T_C = 850^\circ\text{K}$ ).   |
| Ulvöspinel<br>$\text{Fe}_2\text{TiO}_4$                    | Cubic<br>Fd3m<br>$a = 8.538\text{Å}$   | 15.6 (3)  | Polishing hardness < ilmenite |                            |   |   |   |
| Chromite<br>$\text{FeCr}_2\text{O}_4$                      | Cubic<br>Fd3m<br>$a = 8.36\text{Å}$  | 11.5  | 1288-1561                     |                            | =340 kcal/mole  |   | Semiconductor. Ferrimagnetic below $T_C = 90^\circ\text{K}$ .   |
| Wüstite<br>$\text{FeO}$<br>(or $\text{Fe}_{1-x}\text{O}$ ) | Cubic<br>Fm3m<br>$a = 4.307\text{Å}$   | ? less than magnetite                           | ?                             | 1650                       | "FeO" = -65.2 kcal/gfw<br>[Fe <sub>0.947</sub> O] = -63.64 kcal/gfw | "FeO" = -60.01 kcal/gfw<br>[Fe <sub>0.947</sub> O] = -58.6 kcal/gfw | Semiconductor. Antiferromagnetic $T_N \approx 198^\circ\text{K}$ .  |
| Rutile<br>$\text{TiO}_2$                                   | Tetrag.<br>P4 <sub>2</sub> /mmm<br>$a = 4.5933\text{Å}$<br>$a = 2.9592\text{Å}$  | $R_{\text{Fe}} = 19.5$<br>$R_{\text{O}} = 22.8$ | 920-974                       | 2103                       | -255.7 kcal/gfw   | -212.6 kcal/gfw   | Wide band gap semiconductor. Diamagnetic.   |
| Eskolaite<br>$\alpha\text{-Cr}_2\text{O}_3$                | Trig.<br>R3c<br>$a = 4.954\text{Å}$<br>$a = 13.584\text{Å}$  | $R_{\text{Fe}} = 18.2$<br>$R_{\text{O}} = 19.8$ | 2239-2898                     | 2603                       | -272.7 kcal/gfw   | -253.2 kcal/gfw   | Wide band gap semiconductor. Antiferromagnetic $T_N = 308^\circ\text{K}$ .  |

(1) JCPDS Data Book (1974); (2) COM International Tables, Barcelona (1970); (3) Cameron (1970); (4) Robie & Waldbaum (1968); (5) From the compilations of Goodenough (1963, 1971).

corundum. The metals are in octahedral coordination in an approximately hexagonal close-packed array of oxygens: ilmenite differs in having distorted oxygen layers (Table 2).

Molecular orbital calculations utilizing the SCF- $X_\alpha$  scattered wave method have been performed for metal-oxygen polyhedral clusters containing  $\text{Fe}^{3+}$ ,  $\text{Fe}^{2+}$  and  $\text{Ti}^{4+}$  in octahedral coordination to oxygen (Tossell *et al.* 1973, 1974). These calculations were used to model the electronic structures of rutile, wüstite and hematite and to assign and interpret their X-ray and *uv* photoelectron, X-ray emission and absorption, and optical absorption and reflectance spectra. The good agreement between calculated and

observed transition energies support the validity of the calculations. It should be noted, however, that in these calculations, the choice of certain initial parameters employed may affect the results obtained. For example, the use of overlapping spheres defining the various regions around the atoms in the clusters affects ligand *p*-metal 3*d* energy separations by as much as 1 eV (Rösch *et al.* 1973).

The same calculations have been used here to construct schematic ("one-electron") MO/band theory energy-level diagrams for hematite and ilmenite, shown in Figure 1. It has been argued by Goodenough (1963, 1971) that the outermost electrons in the valence region for these mate-

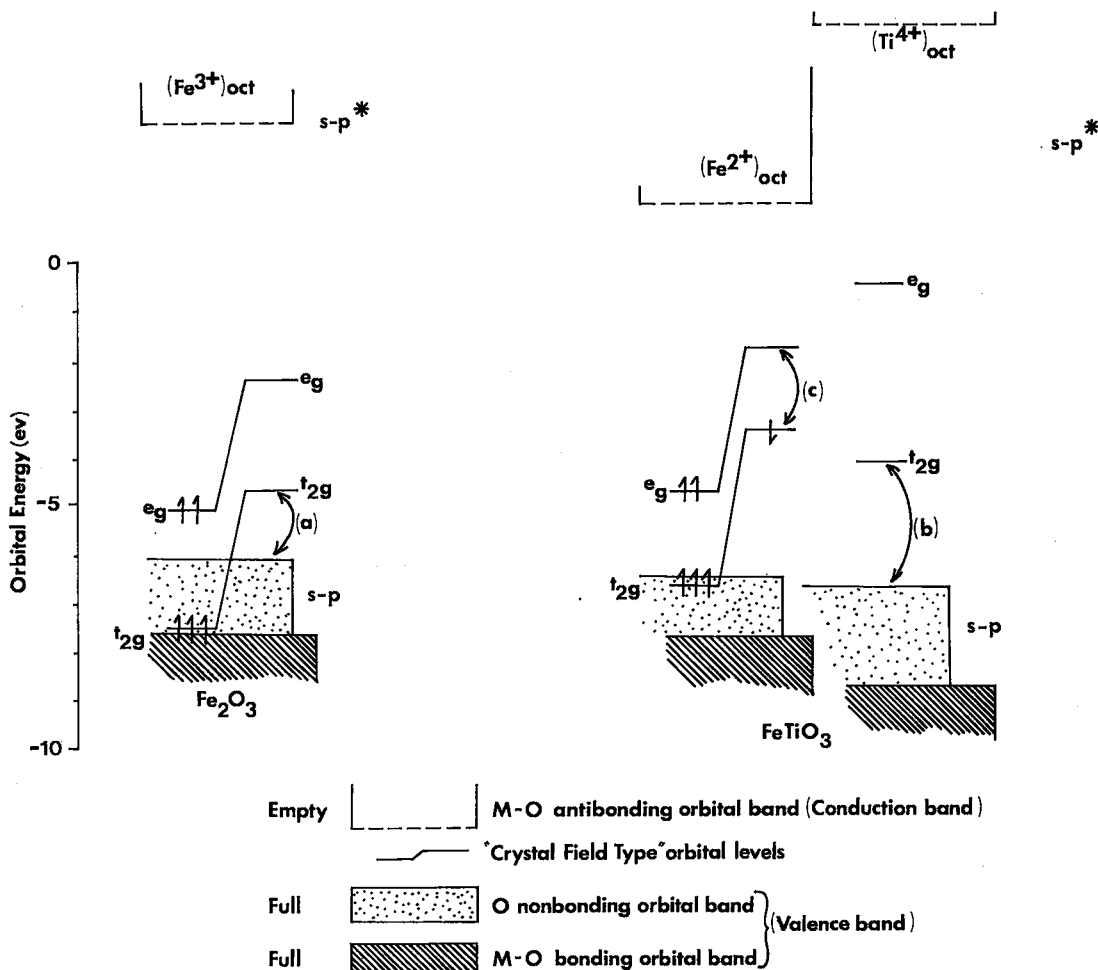


FIG. 1. Molecular orbital/band models to illustrate the electronic structures of hematite and ilmenite. Calculations were performed on an  $\text{FeO}_6^{9-}$  cluster at an Fe-O distance of 2.06 Å (as in  $\text{Fe}_2\text{O}_3$ ), a  $\text{FeO}_6^{10-}$  cluster at an Fe-O distance of 2.17 Å (*cf.*, 2.14 Å in  $\text{FeTiO}_3$ ) and  $\text{TiO}_6^{9-}$  cluster at a Ti-O distance of 1.965 Å (*cf.*, 1.98 Å in  $\text{FeTiO}_3$ ).

rials may be described using localized models. Hence the orbitals, dominantly of metal  $3d$  character, are shown in the diagram as discrete levels, whereas the other levels are shown as broadening into bands.

As this is the first of the energy-level diagrams, more detailed discussion is appropriate. The diagram shown for hematite in Figure 1 has many features in common with the familiar MO diagrams of elementary chemistry texts (Gray 1965; Cotton & Wilkinson 1972). One complexity immediately seen is the effect of unpaired spins on the electrons of the partly filled  $3d$  orbitals in splitting the valence-orbital energy levels into "spin-up" ( $\uparrow$ ) and "spin-down" ( $\downarrow$ ) levels. From the calculations, it is also possible to comment on the composition of particular molecular orbitals in terms of the contribution of atomic orbitals of metal or oxygen. In the  $\text{FeO}_6^{4-}$  cluster of hematite, the highest-energy filled orbital is an  $e_g\uparrow$  orbital that is antibonding in character (mainly  $\text{Fe}3d$  and  $\text{O}2p$ ). The filled  $t_{2g}\uparrow$  orbital (a bonding orbital of  $\text{Fe}3d$  and  $\text{O}2p$  character) lies several eV lower in energy, beneath energy levels shown at the top of a delocalized band in Figure 1. As in all of the oxide systems studied, the top of this  $s-p$  band is made up of  $\text{O}2p$  non-bonding orbitals. Several eV below the top of this band are the main bonding orbitals of  $\text{Fe}3d$ ,  $4s$ ,  $4p$  and  $\text{O}2p$  character. The vacant orbitals in the valence region are the  $e_g\downarrow$  and  $t_{2g}\downarrow$  shown in Figure 1, and (about 9 eV above the highest filled orbital) the diffuse antibonding orbitals of the  $s-p^*$  band with metal and oxygen  $s$  and  $p$  orbital character.

One weakness of these calculations is their failure to accurately reproduce the energy separation of the  $3d$  orbital energy levels when split by the octahedral crystal field. However, Sambe & Felton (1976) have shown that values of crystal field splitting ( $10Dq$ ) are more accurately reproduced in SCF- $X_\alpha$  calculations by using the transition-state procedure in which half an electron is transferred from the ground state to the excited state and the calculation reiterated to self-consistency. When there is spin-splitting of the valence orbital energy levels,  $10Dq$  should be the average of the separations of "spin-up" and "spin-down"  $t_{2g}$  and  $e_g$  levels calculated by the transition-state procedure. Using the above procedure,  $10Dq$  values from the SCF- $X_\alpha$  calculations are found to be in better agreement with experiment than had been previously assumed (Vaughan *et al.* 1974).

In Figure 1, a similar model for ilmenite is based on calculations on the  $\text{FeO}_6^{3-}$  and  $\text{TiO}_6^{3-}$  clusters. The nature of the  $s-p$  (bonding) and

$s-p^*$  (antibonding) bands is much the same as in  $\text{Fe}_2\text{O}_3$ . However, the  $3d$  levels of  $\text{Fe}^{2+}$  do not overlap the  $s-p$  band as much and, along with the vacant  $\text{Ti}3d$  levels, there is the additional  $t_{2g}\downarrow$  electron of  $\text{Fe}^{2+}$ . The vacant  $t_{2g}$  and  $e_g$  levels of  $\text{TiO}_6^{3-}$  have both  $\text{Ti}3d$  and  $\text{O}2p$  character, with the  $e_g$  level of antibonding character.

Reference to Table 1 shows that the calculated  $t_{2g}-e_g$  separation (crystal-field splitting) exceeds that found experimentally using spectroscopic data and adjustment should be made for this. Although both hematite and ilmenite are antiferromagnetic at  $25^\circ\text{C}$ , the coupling energies involved in these interactions between polyhedra are only fractions of an eV and can be ignored for these and the spinel compounds in the present models.

### Interpretation of properties

The properties of hematite and ilmenite, summarized in Table 2, will now be considered using the models outlined and also noting data from Table 1. Electrical and magnetic studies (Table 2) show that both oxides are essentially semiconducting antiferromagnetic compounds at low temperatures, with their outermost ( $3d$ ) electrons localized on the cations and unpaired electrons on adjacent metals coupled antiparallel. The electrical conductivities (or resistivities) of the pure oxides are difficult to define because of the large effects of minor impurities or deviations from stoichiometry. However, the simple models of Figure 1 indicate a smaller separation between occupied and unoccupied energy levels in hematite than in ilmenite, which should indicate a significantly lower resistivity. Available data confirm that the intrinsic resistivity of hematite is  $\sim 0.3$  ohm-m, whereas that of ilmenite is  $\sim 0.8-1.8$  ohm-m (Shuey 1975).

The optical properties of greatest mineralogical interest are the spectral reflectance values throughout the visible region of the spectrum. Detailed data for hematite, ilmenite and a titanium-bearing hematite have been reported by von Gehlen & Piller (1965) between 440 and 660nm. Values for the two principal vibration directions in plane-polarized light are shown (Fig. 2) for both pure hematite and pure ilmenite. Burns & Vaughan (1970) and Vaughan (1973, 1975) have argued that high reflectance values result from excitation and delocalization of electrons into orbitals or bands of diffuse, antibonding (*i.e.*, "conduction band") character. Examination of the electronic-structure models (Fig. 1) shows that "allowed" electronic transitions occur in ilmenite from mainly oxygen  $s-p$  to titanium  $t_{2g}$  orbitals at an energy correspond-

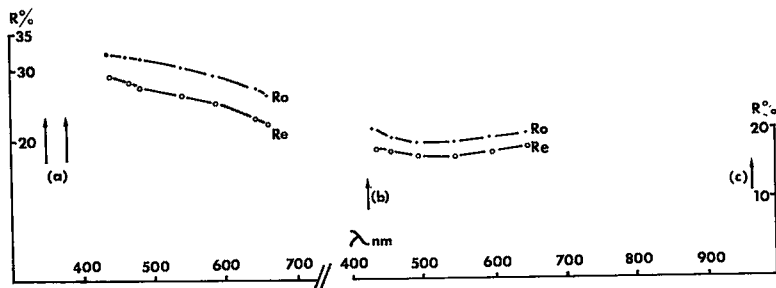


FIG. 2. Spectral reflectivity data in the visible light range ( $\sim 400\text{--}700\text{nm}$ ) for hematite (left) and ilmenite (right). Data are shown for both the ordinary ( $R_o$ ) and extraordinary ( $R_e$ ) vibration directions in plane-polarized light; arrows indicate the energy regions of the major electronic transitions.

ing to  $\sim 400\text{nm}$  as indicated by the labels in Figures 1 and 2. "Allowed" transitions also occur from iron  $t_{2g} \downarrow$  to  $e_g \downarrow$  orbitals at energies corresponding to  $\sim 1000\text{nm}$ . These transitions, corresponding to the absorption and subsequent re-emission of energy, account for the higher values of reflectance at either end of the  $\sim 400\text{--}700\text{nm}$  profile. In hematite, the  $s\text{--}p \rightarrow t_{2g}$  transitions at an energy corresponding to  $\sim 400\text{nm}$  account for the decrease in reflectance from  $400 \rightarrow 700\text{nm}$ , and the greater concentration of iron contributing to this transition, for the greater overall reflectance.

Calculations on an octahedral  $\text{TiO}_6^{9-}$  cluster using the same methods (Loeffler *et al.* 1974) show that  $\text{Ti}^{3+}$  substitution in ilmenite should introduce a positive feature at  $\sim 530\text{nm}$  in the spectral profile. As  $\text{Ti}^{3+}$  ions are postulated to occur in lunar ilmenites, it is particularly interesting that such a feature has been tentatively observed in spectral reflectance measurements of some of the lunar ilmenites (Simpson & Bowie 1970).

The Vickers microhardness data show a marked decrease in mean values from hematite to ilmenite ( $926 \rightarrow 626$ ; see Table 2) which can be correlated with an increase in the unit-cell dimensions of 1% in the  $a$  parameter and 2% in the  $c$  parameter (Table 2). The major contribution to this is the additional  $t_{2g} \downarrow$  electron of  $\text{Fe}^{2+}$  (which consequently has a 20% greater ionic radius; Table 1).

Although hematite and ilmenite are very similar in crystal structures, the differences in electronic structure are sufficient to greatly limit solid solution between them at room temperature (Nicholls 1955). Above  $1050^\circ\text{C}$ , there is complete solid solution between hematite and ilmenite but at  $800^\circ\text{C}$ , not more than 5%  $\text{TiO}_2$  can

enter the  $\alpha\text{-Fe}_2\text{O}_3$  structure.

The thermochemical data (Table 2) show a considerable difference in the free energies of formation of hematite and ilmenite, and a number of observations can be made regarding this difference. The crystal-field-theory approach would emphasize the stabilization gained by the addition of the sixth  $3d$  electron of  $\text{Fe}^{2+}$  (Table 1). Reference to the MO model (Fig. 1) emphasizes another important factor. Although the energies of  $\text{Fe}^{3+}\text{--O}$  and  $\text{Fe}^{2+}\text{--O}$  bonding orbitals are very similar, the  $\text{Ti}^{4+}\text{--O}$  bonding orbital set is stabilized (by  $\sim 1\text{ eV}$ ) relative to the iron-oxygen bonds. This very important contribution to the stability of ilmenite relative to hematite is, of course, not considered in crystal-field theory. Another consequence of this difference in electronic structure has been noted by Gaffney & Ahrens (1970) who used an electrostatic model to calculate enthalpies of formation of oxide minerals. The discrepancy between calculated and measured enthalpies was much greater for oxides containing octahedral  $\text{Ti}^{4+}$  than  $\text{Fe}^{3+}$  or  $\text{Fe}^{2+}$ , and was attributed to a covalency effect.

#### THE SPINEL OXIDES: CHROMITE, MAGNETITE AND ULVÖSPINEL

The spinel crystal structure, common to these three important oxide minerals, is illustrated in Figure 3. Whereas chromite is a normal spinel with nominally divalent ions ( $\text{Fe}^{2+}$ ) in the tetrahedral sites and trivalent ions ( $\text{Cr}^{3+}$ ) in octahedral sites, *i.e.*,  $\text{Fe}^{2+}(\text{Cr}^{3+}\text{Cr}^{3+})\text{O}_4$ , magnetite is an inverse spinel, *i.e.*,  $\text{Fe}^{3+}(\text{Fe}^{2+}\text{Fe}^{3+})\text{O}_4$ . Ulvöspinel is unusual in containing tetravalent ions, *i.e.*,  $\text{Fe}^{2+}(\text{Fe}^{2+}\text{Ti}^{4+})\text{O}_4$ .

In addition to the molecular orbital calculations (using the SCF- $X_\alpha$  method) already men-

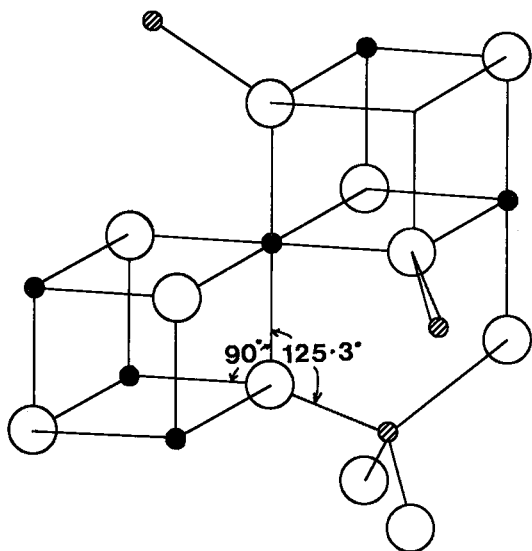


FIG. 3. The crystal structure of a spinel ( $AB_2O_4$ ).

tioned, similar calculations have also been performed for an  $FeO_4^{6-}$  tetrahedral cluster (Vaughan *et al.* 1974), a  $CrO_6^{9-}$  octahedral cluster (Tossell & Vaughan, unpubl.; Tossell 1976b), and an  $FeO_4^{5-}$  cluster (Tossell 1978). Using combined data from all of these calculations, it has been possible to construct the schematic energy level diagrams illustrated in Figure 4. Again, the electrical and magnetic data show that the outermost (dominantly metal 3d) electrons are localized on the cations (Table 2).

Chromite combines the results of tetrahedral  $FeO_4^{6-}$  cluster and octahedral  $CrO_6^{9-}$  cluster calculations as shown in Figure 4A. Here, the  $FeO_4^{6-}$  empty conduction-band orbitals have metal and oxygen character and the crystal-field type  $e\uparrow$  orbital is mostly  $Fe3d$ . The empty  $t_2\downarrow$  orbital is also dominantly  $Fe3d$ , but with some 4p character, whereas the  $t_2\uparrow$  orbital is equally oxygen p and  $Fe3d$  with some 4p. As in other systems studied, the orbitals immediately beneath these in energy are almost totally oxygen (nonbonding) in character. A similar overall structure is indicated by the calculations on  $CrO_6^{9-}$ . Here, both  $e_g$  orbitals exhibit appreciable oxygen as well as chromium character and the  $t_{2g}$  orbitals rather less oxygen character.

Magnetite can be modelled using the results of cluster calculations on  $FeO_4^{5-}$ ,  $FeO_6^{10-}$  and  $FeO_6^{9-}$  as shown in Figure 4C. The valence region X-ray and *uv* photoelectron spectra of magnetite can be correlated with the results of these calculations (Tossell 1978). The atomic orbital compositions of the molecular orbitals for the octahedral-site ions can be regarded as similar to those

described for hematite and ilmenite. The tetrahedrally coordinated  $Fe^{3+}$  is similar to tetrahedrally coordinated  $Fe^{2+}$  in having the crystal-field type levels above and separate from the oxygen nonbonding set and the main Fe-O bonding orbitals of the system. Spin-splitting of the orbitals is not quite so large in  $Fe^{2+}$ .

In the case of ulvöspinel, the  $FeO_6^{10-}$  and  $TiO_6^{8-}$  octahedral cluster calculations can again be used and, combined with the calculation on  $FeO_4^{6-}$  in tetrahedral coordination, result in the model shown in Figure 4B.

#### Interpretation of properties

The optical properties of these three spinel oxides are shown in the spectral reflectance profiles of Figure 5 and the numerical data of Table 2. Certain of the 'allowed' transitions described for hematite and ilmenite are applicable to some of the spinel oxides and the additional transitions have been labelled in Figure 5 and inserted in Figure 4. Following similar arguments to those used in the discussion of hematite and ilmenite, the reflectance profiles shown for these minerals can also be interpreted in terms of electronic structure.

In chromite, which shows the lowest overall reflectance, the transition chiefly contributing to the reflectance is the 'spin-allowed' crystal-field transition in the octahedral  $Cr^{3+}$  ions (labelled (f) in Figures 4A and 5) at  $\sim 530$  nm. This also contributes to the higher reflectance at the 400nm end of the spectrum in this mineral. The ulvöspinel reflectance profile resembles that of ilmenite since the same 'allowed' transitions in octahedral  $Fe^{2+}$  and  $Ti^{4+}$  ions contribute to the higher reflectance values towards either end of the visible range. Magnetite, showing the highest overall reflectance values, has contributions from oxygen  $\rightarrow$  metal charge-transfer transitions [(a) and (d) in Figures 4C and 5] and the spin-allowed crystal-field transition in octahedral  $Fe^{2+}$  [(c) in Figures 4C and 5].

Complete Vickers microhardness data are not available for these three minerals (Table 2) but available information suggests that chromite is much harder than the other two spinels. This correlates with the small unit-cell parameter and absence of electrons in the  $e_g$  orbital levels in the octahedral sites. On the basis of the cell parameter data (Table 2), the  $e_g\downarrow$  electron of octahedral  $Fe^{2+}$  and  $t_2\downarrow$  electron of tetrahedral  $Fe^{2+}$ , ulvöspinel is predicted to be the softest of these three spinel phases (*i.e.*,  $VHN \leq 530$ ).

Thermochemical data are also incomplete for these three spinels (Table 2) but chromite probably has a significantly greater value for  $\Delta G^\circ_{298}$

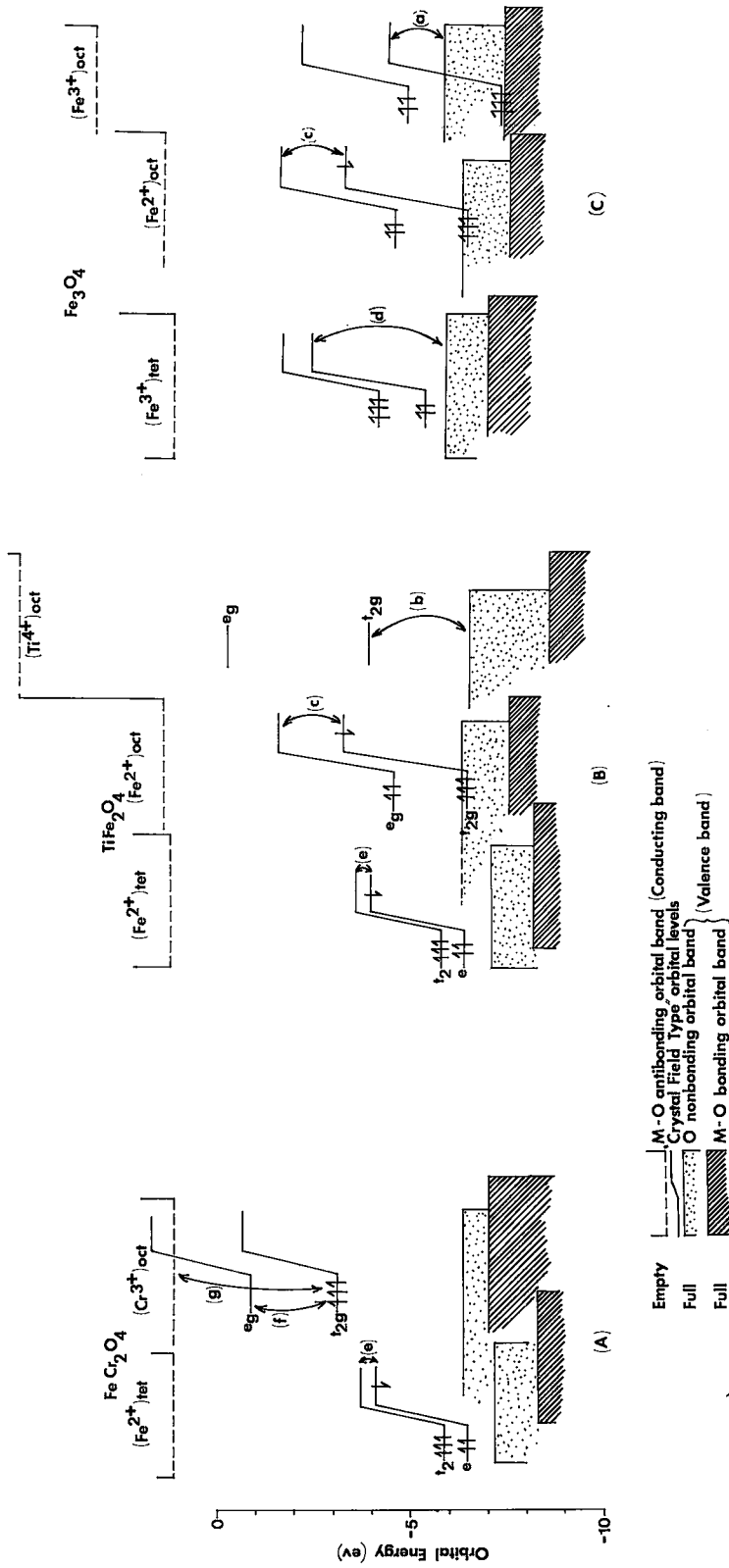


Fig. 4. Molecular orbital/band models to illustrate the electronic structures of chromite, ulvöspinel and magnetite. Models employ data from the  $\text{FeO}_6^{4-}$ ,  $\text{FeO}_6^{3-}$ ,  $\text{TiO}_6^{3-}$  clusters as in Figure 1 and from calculations on  $\text{FeO}_4^{2-}$  (at Fe-O distance of 1.99Å),  $\text{FeO}_6^{4-}$  (Fe-O of 1.89Å) and  $\text{CrO}_6^{3-}$  (at Cr-O of 2.00Å).

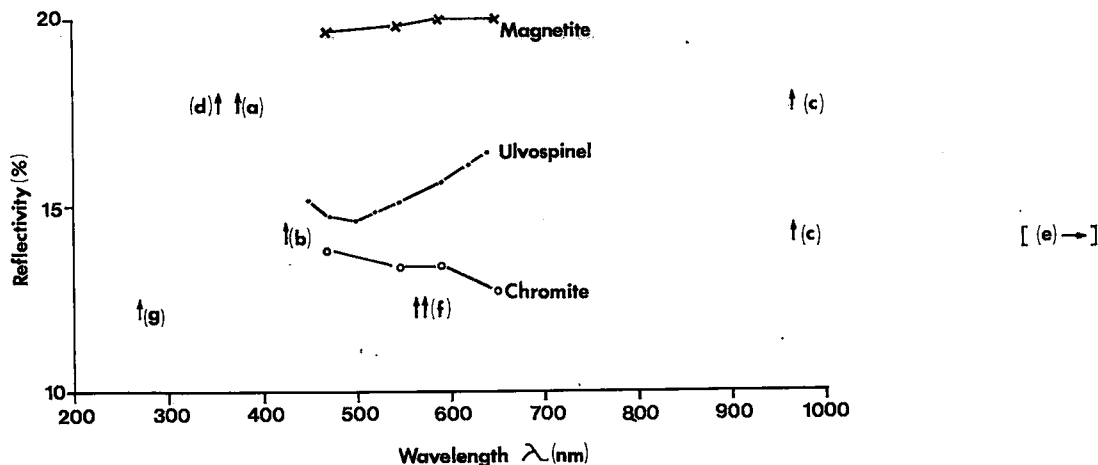


Fig. 5. Spectral reflectivity data in the visible light range for chromite, ulvöspinel and magnetite. Arrows indicate energies of the major electronic transitions.

than magnetite. In terms of crystal-field theory, these data could be interpreted as due to the considerable stabilization of  $\text{Cr}^{3+}$  in octahedral sites. The MO model (Fig. 4A) suggests that this may be partly compensated for by lesser stabilization of metal-oxygen bonding interactions than in octahedrally coordinated  $\text{Fe}^{2+}$ ,  $\text{Fe}^{3+}$  or  $\text{Ti}^{4+}$ . Although ulvöspinel (Fig. 4B) has an additional  $e \downarrow$  electron which is antibonding in character, the metal-oxygen bonding orbitals are all stabilized relative to those in magnetite so that the value of  $\Delta G^{\circ}_{298}$  may well be greater than that of magnetite.

#### WÜSTITE, RUTILE AND ESKOLAITE

The binary oxides wüstite, rutile and eskolaite, although not of equal petrological importance, complete this discussion of the electronic structures of oxide minerals. The crystal structures of wüstite and rutile (Table 2) are distinct from the other minerals considered; eskolaite, like hematite, has the corundum structure.

The electronic structures of these three minerals can be described with energy-level diagrams constructed from molecular orbital calculations which have already been discussed (*i.e.*,  $\text{FeO}_6^{10-}$ ,  $\text{TiO}_6^{8-}$ ,  $\text{CrO}_6^{9-}$ ). The diagrams are illustrated in Figure 6 and the molecular orbital compositions in terms of atomic orbital contributions are as already outlined.

#### Interpretation of properties

Spectral reflectance data are shown for rutile and eskolaite in Figure 7. A number of the elec-

tronic transitions outlined in the discussion of the ilmenite and chromite spectra are invoked to interpret these data. The higher reflectance of rutile at the 400nm end of the spectrum is attributed to the oxygen  $\rightarrow$  metal charge-transfer transition labelled (b), whereas in eskolaite, both the spin-allowed  $t_{2g} \rightarrow e_g$  transition (f) and the  $t_{2g} \rightarrow$  conduction-band transition (g) contribute to increased reflectance towards 400nm. The energy of transition (f) is probably slightly underestimated and may be at a rather shorter wavelength.

Vickers hardness data, also available only for rutile and eskolaite, indicate that eskolaite is much harder. It is also the most stable of the three oxides, with the largest negative free energy of formation. Thus, the contribution to bond strength of the three  $t_{2g} \uparrow$  electrons is considerable and outweighs the slight destabilization of the  $M-O$  bonding orbital band relative to  $\text{TiO}_2$ . In  $\text{FeO}$ , the least stable and probably the softest of the three oxides, the destabilizing effect of the  $t_{2g} \downarrow$  electron is not offset by any gain in  $M-O$  bonding orbital energies. From the complex and incomplete data on the electrical properties of these binary oxides it may be noted that "pure" rutile has an extremely high resistivity ( $\sim 10^7$  ohm-m; Shuey 1975), as would be expected from the large separation of occupied and unoccupied orbitals.

#### DISCUSSION

Quantitative "one-electron" models of the electronic structures of the major transition-

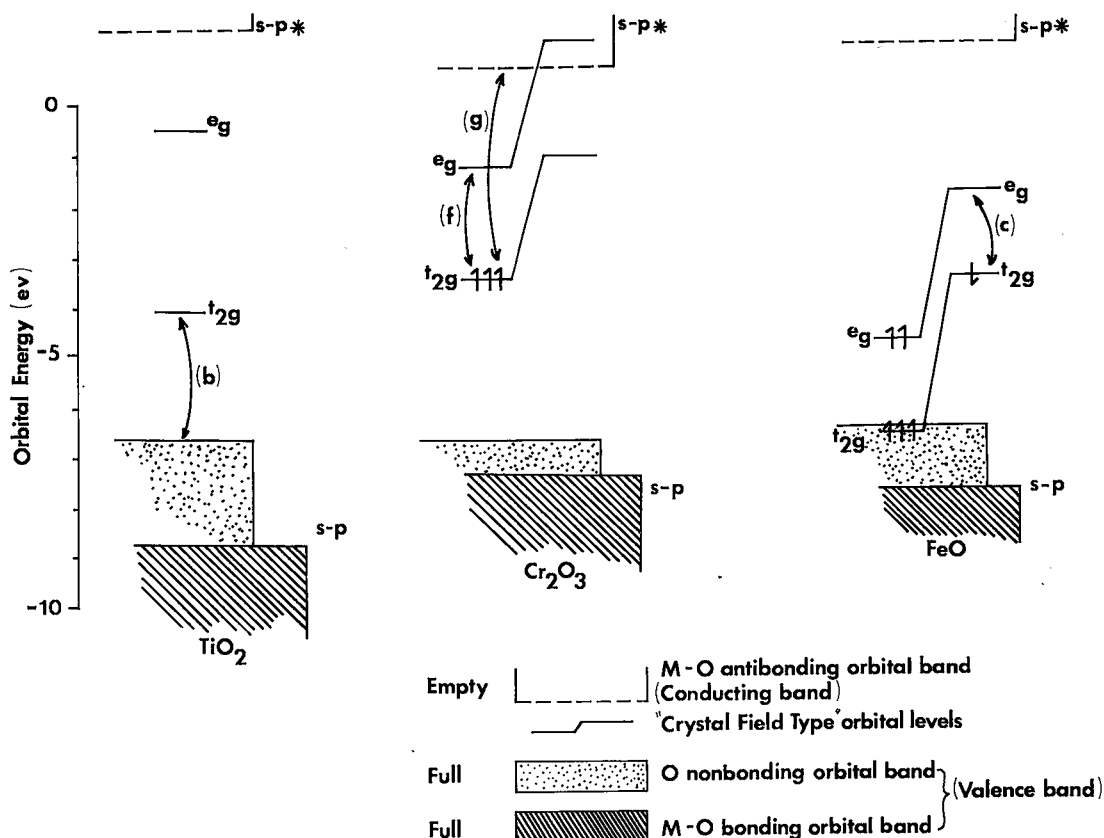


FIG. 6. Molecular orbital/band models to illustrate the electronic structures of rutile, eskolaite and wüstite. Data from same calculations as in Figure 4.

metal oxide minerals have been presented and correlated with the properties of these minerals.

The models represent a quantification of the type of MO/band theory approach used by Goodenough (1963, 1971) and are currently the most satisfactory simplified approach to an understanding of these complex materials.

Further calculations and spectroscopic measurements will enable refinement of these models. Also, calculations at reduced internuclear distances will permit assessment of the effects of pressure on electronic structure, and hence, properties. Such studies of iron-oxygen clusters (Tossell 1976a) indicate large changes in bond character for compressed iron oxides.

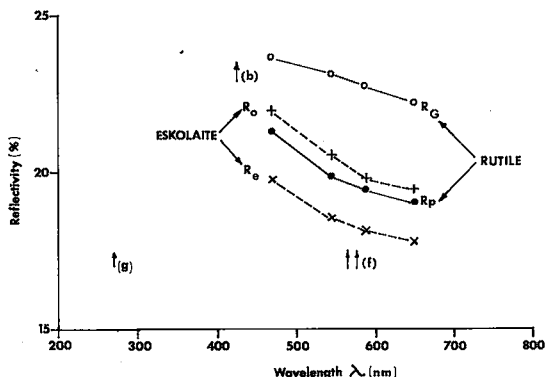


FIG. 7. Spectral reflectivity data in the visible light range for rutile and eskolaite. Arrows indicate energies of the major electronic transitions.

ACKNOWLEDGEMENTS

Dr. D. J. Vaughan acknowledges the support of a grant from the North Atlantic Treaty Organization which helped in the completion of this work, and the editorial assistance of Mrs. H. E. Vaughan. Dr. J. A. Tossell acknowledges

support from the donors of the Petroleum Research Fund, administered by the American Chemical Society. Mrs. P. Minor is thanked for the preparation of the typescript and Miss B. A. Parker for the preparation of the diagrams.

## REFERENCES

- BERRY, L. G. ed. (1974): *Selected Powder Diffraction Data for Minerals*. Publ. M-1-23, Joint Committee on Powder Diffraction Standards, Swarthmore, Pa.
- BURNS, R. G. (1970): *Mineralogical Applications of Crystal Field Theory*. Cambridge University Press, Cambridge.
- & VAUGHAN, D. J. (1970): Interpretation of the reflectivity behavior of ore minerals. *Amer. Mineral.* 55, 1576-1586.
- CAMERON, E. N. (1970): Opaque minerals in certain lunar rocks from Apollo 11. *Proc. 1st Lunar Sci. Conf.* 1, 221-245.
- COMMISSION ON ORE MICROSCOPY (1970): *International Tables for the Microscopic Determination of Crystalline Substances Absorbing in Visible Light*. (provisional issue) Barcelona.
- COTTON, F. A. & WILKINSON, G. (1972): *Advanced Inorganic Chemistry*, 3rd ed. Interscience, New York.
- GAFFNEY, E. S. & AHRENS, T. J. (1970): Stability of mantle minerals from lattice calculations and shock wave data. *Phys. Earth. Planet. Int.* 3, 205-212.
- GOODENOUGH, J. B. (1963): *Magnetism and the Chemical Bond*. Interscience, New York.
- (1971): Metallic oxides. In *Progress in Solid-State Chemistry* 5 (H. Reiss, ed.), Pergamon, Oxford.
- GRAY, H. B. (1965): *Electrons and Chemical Bonding*. Benjamin, New York.
- LOEFFLER, B. M., BURNS, R. G., TOSSELL, J. A., VAUGHAN, D. J. & JOHNSON, K. H. (1974): Charge transfer in lunar materials: interpretation of ultraviolet-visible spectral properties of the moon. *Proc. 5th Lunar Sci. Conf.* 3, 3007-3016.
- MAO, H. K. & BELL, P. M. (1975): Crystal-field effects in spinel: oxidation states of iron and chromium. *Geochim. Cosmochim. Acta* 39, 865-874.
- NICHOLLS, G. D. (1955): The mineralogy of rock magnetism. *Adv. Phys.* 4, 113-190.
- ROBIE, R. A. & WALDBAUM, D. R. (1968): Thermodynamic properties of minerals and related substances at 298.15K and one atmosphere pressure and at higher temperatures. *U.S. Geol. Surv. Bull.* 1259.
- RÖSCH, N., KLEMPERER, W. G. & JOHNSON, K. H. (1973): On the use of overlapping spheres in the SCF  $X_{\alpha}$  scattered-wave method. *Chem. Phys. Lett.*, 23, 149-154.
- SAMBE, H. & FELTON, R. H. (1976): Connection between the  $X_{\alpha}$  method and ligand field theory. *Int. J. Quant. Chem. Symp.* 10, 155-158.
- SHANNON, R. D. (1976): Revised effective ionic radii and systematic studies of interatomic distances in halides and chalcogenides. *Acta Cryst.* A32, 751-767.
- SHUEY, R. T. (1975): *Semiconducting Ore Minerals*. Developments in Economic Geology 4, Elsevier, Amsterdam.
- SIMPSON, P. R. & BOWIE, S. H. U. (1970): Quantitative optical and electron-probe studies of opaque phases in Apollo 11 samples. *Proc. 1st Lunar Sci. Conf.* 1, 873-890.
- TOSSELL, J. A. (1976a): Electronic structures of iron-bearing oxidic minerals at high pressure. *Amer. Mineral.* 61, 130-144.
- (1976b): The electronic structures of the core and valence ion states of metal oxides. *J. Electron Spectrosc. relat. Phenom.* 8, 1-14.
- (1978): Self-consistent field  $X_{\alpha}$  study of one-electron energy levels in  $Fe_3O_4$ . *Phys. Rev. B* (in press).
- , VAUGHAN, D. J. & JOHNSON, K. H. (1973): Electronic structure of ferric iron octahedrally coordinated to oxygen. *Nature Phys. Sci.* 244, 42-45.
- , ——— & ——— (1974): The electronic structure of rutile, wüstite and hematite from molecular orbital calculations. *Amer. Mineral.* 59, 319-334.
- VAUGHAN, D. J. (1973): Spectral reflectance properties of minerals and their interpretation. *Mineral. Mater. News Bull. Quant. Microsc. Methods* 3, 9-11; 4, 14-15.
- (1975): Further discussion on the origin of spectral reflectance variation in ore minerals. *Mineral. Mater. News Bull. Quant. Microsc. Methods* 2, 7-8; 3.
- , TOSSELL, J. A. & JOHNSON, K. H. (1974): The bonding of ferrous iron to sulfur and oxygen in tetrahedral coordination: a comparative study using SCF  $X_{\alpha}$  scattered wave molecular orbital calculations. *Geochim. Cosmochim. Acta* 38, 993-1005.
- VON GEHLEN, K. & PILLER, H. (1965): Zur Optik von Hämatit und Ilmenit. *Neues Jahrb. Mineral. Monatsh.*, 97-108.

Received August 1977; revised manuscript accepted November 1977.